Journal of Alloys and Compounds 509 (2011) 10217–10221

Contents lists available at SciVerse ScienceDirect

Journal of Alloys and Compounds

journal homepage: www.elsevier.com/locate/jallcom

# Microstructure and thermoelectric properties of β-$FeSi_2$ ceramics fabricated by hot-pressing and spark plasma sintering

Xiurong Qu*, Shuchen Lü, Jianmin Hu, Qingyu Meng

*Heilongjiang Key Laboratory for Low Dimensional System and Mesoscopic Physics, School of Physics and Electronic Engineering, Harbin Normal University, Harbin, 150025, China*

ARTICLE INFO

*Article history:*
Received 9 May 2011
Received in revised form 16 August 2011
Accepted 17 August 2011
Available online 25 August 2011

*Keywords:*
Thermoelectric materials
Ceramics
Mechanical alloying
Sintering

ABSTRACT

The microstructure and thermoelectric properties of β-$FeSi_2$ ceramics by hot pressing (HP) and spark plasma sintering (SPS) are investigated. With increasing hot-pressing temperature, the density, electronic conductivity and thermal conductivity of the samples increase significantly, the thermoelectric figure of merit is improved slightly. The microstructure study indicates that the sizes of the β-$FeSi_2$ and ε-FeSi phases in the sample sintered by the SPS process are smaller than that by the HP process. The SPS sample shows excellent thermoelectric performance due to the low thermal conductivity.

© 2011 Elsevier B.V. All rights reserved.

## 1. Introduction

Thermoelectric (TE) apparatus plays an important role in energy crisis. As well known, the high TE conversion efficiency strongly depends on the performance of TE materials, which is denoted by the TE figure of merit of the materials [1,2]. The figure of merit is defined as $ZT = \alpha^2\sigma T/\kappa$, where $T$ is absolute temperature, $\sigma$ is the electrical conductivity, $\alpha$ is the Seebeck coefficient, and $\kappa = \kappa_l + \kappa_e$ is the thermal conductivity composed of electronic and lattice parts [3,4]. Thus, excellent TE materials impose high $\sigma$, high $\alpha$ and low $\kappa$.

As one of the most important semiconductor materials, β-$FeSi_2$ has a band gap of 0.85 eV at room temperature, and has large Seebeck coefficient ($\alpha$) [5]. Furthermore, owing to the non-toxicity and storage of the constituent elements of β-$FeSi_2$, much attention is attracted to realize its application in thermo-generators [6,7]. Nevertheless, the high thermal conductivity $\kappa$ of β-$FeSi_2$ based alloys leads to a low figure of merit. To enhance the figure of merit of β-$FeSi_2$ based materials, many research efforts have been tried, such as solid solution formation, fine particle dispersion, and grain refinement [8,9].

Rapid solidification followed by hot pressing is found to be an effective way to produce fine grain structures, and improve the phase transformation speed and the TE properties for iron disilicide. However, the fine grain sizes in these alloys grow rapidly up to about 5 μm after hot pressing at 975 °C under 50 MPa for 30 min [10]. This is possible because of the low heating rates used and long sintering time is required to obtain full dense ceramics. Fortunately, the recent use of spark plasma sintering has provided many successful examples in the preparation of highly dense nanostructured ceramics [3,11]. This technique offers a unique combination of rapid heating/cooling and shorter processing time, which makes it consolidate nanopowders and retain nanostructures [12]. For example, Guo et al. have reported that hot pressing (HP) and spark plasma sintering (SPS) led to the appearance of different secondary phases in $ZrB_2$–SiC ceramics with $Yb_2O_3$ additive. Hot-pressed $ZrB_2$–SiC ceramics with $Yb_2O_3$ additive had coarsened microstructure, and spark plasma-sintered $ZrB_2$–SiC ceramics with $Yb_2O_3$ additive exhibited refined microstructure [13]. Xie et al. have reported that the TE properties of BiSbTe alloys were enhanced remarkably by SPS process in comparison to that by zone melted process [14].

In the present work, we report the preparation and TE characterization of β-$FeSi_2$ materials consolidated by HP and SPS, respectively. The influences of sintering techniques and temperature on microstructure and TE properties were investigated.

## 2. Experimental

The sintered β-$FeSi_2$ ($n$-type $Fe_{0.98}Co_{0.02}Si_2$) samples were fabricated by the following process.

Fe (99.99%), Si (99.95%) and Co (99.99%) powders were mixed to corresponding to compositions of $Fe_{0.98}Co_{0.02}Si_2$. The powder mixtures were loaded into a 250 ml tempered steel vial together with two kinds of tempered steel milling balls, one was 20 mm in diameter and the other was 10 mm in diameter, and their numbers were 4 and 20, respectively. The powder to ball mass ratio is 1:10. The vial was filled with argon and sealed with a flexible O-ring to prevent from being oxidized during milling process. Mechanical alloying was performed for 25 h in a shaker miller (model

---

* Corresponding author. Tel.: +86 451 51713966.
*E-mail address:* quxiurong2002@163.com (X. Qu).

0925-8388/$ – see front matter © 2011 Elsevier B.V. All rights reserved.
doi:10.1016/j.jallcom.2011.08.070

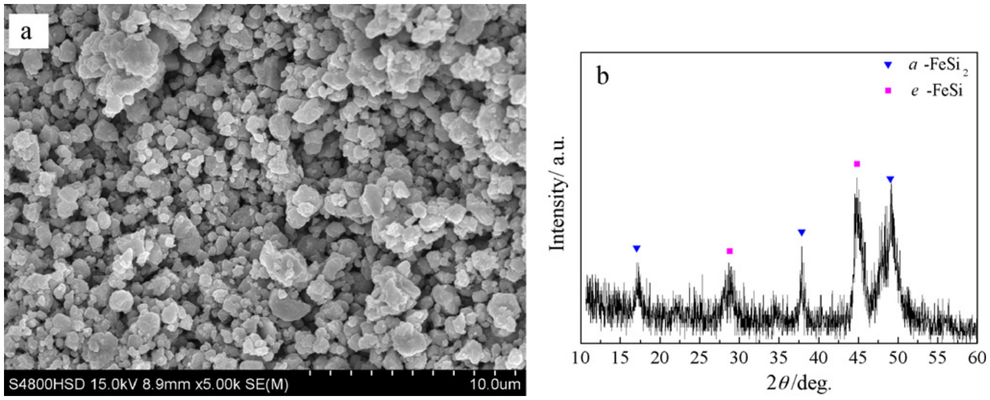

**Fig. 1.** Fe–Si–Co powders milled for 25 h: (a) SEM image; and (b) XRD patterns.

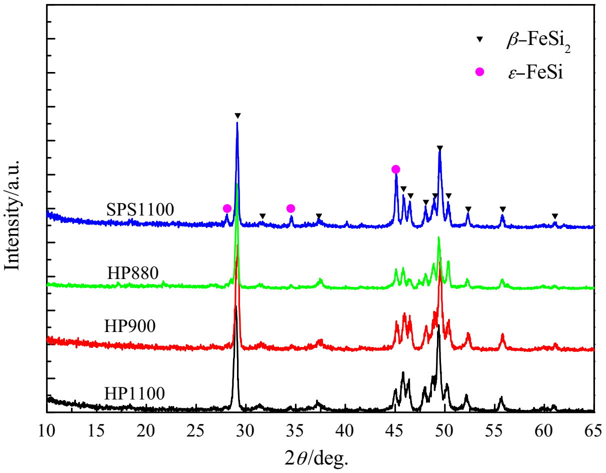

**Fig. 2.** XRD patterns of the HP and SPS samples.

ABQ-045-I, Changjiang Anwei Technology Development Co. Ltd., Changchun, China). To consolidate, the as-milled powders were hot-pressed (Model HPW 150/200-2200-100-LA) at 880 °C, 900 °C and 1100 °C under a pressure of 40 MPa for 30 min in vacuum, respectively. The SPS experiments were performed using an SPS apparatus (SPS-3.20-MK-V, Sumitomo Coal, Japan) without incorporation of any kind of additives at 1100 °C under a constant uniaxial pressure of 40 MPa for 5 min in vacuum. After reactive sintering, the samples were annealed in a vacuum furnace at 800 °C for 5 h to promote the formation of β-FeSi$_2$. The hot-pressed samples were named as HP880, HP900, HP1100, respectively, corresponding to their sintering temperatures. The sample sintered by SPS was marked as SPS1100.

The phase structures of the as-synthesized products were examined by using a powder X-ray diffraction (XRD, Rigaku D/MAX-rB diffractometer with Cu K$\alpha$ ($\lambda$ = 1.5406 Å) radiation operating at 60 kV and 80 mA). The size, morphology and structure of the powder particles were observed by a scanning electron microscope (SEM, S4800) and transmission electron microscopes (Philips CM-12 with an accelerating voltage of 120 kV and Tecnai G2F30 with an accelerating voltage of 300 kV) with attached energy dispersed spectrometer (EDS). The electrical conductivity ($\sigma$) and the Seebeck coefficient ($\alpha$) were simultaneously measured from room temperature to 1200 K using the home-built equipment. The samples for the measurements of electric transport properties were cut out of the sintered bodies in the form of rectangular bars of 2 mm × 2 mm × 20 mm. Electrical conductivity was measured by the ordinary direct current (dc) four-probe method in a flowing argon

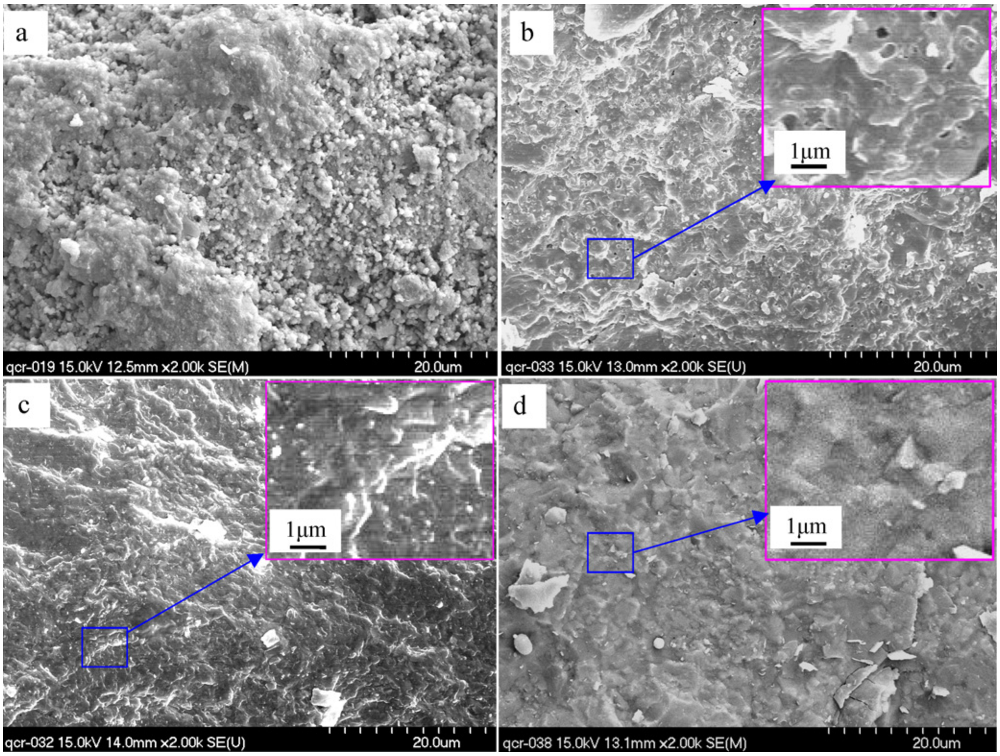

**Fig. 3.** SEM images of the cross-sections of the samples: (a) HP880; (b) HP900; (c) HP1100; and (d) SPS1100.

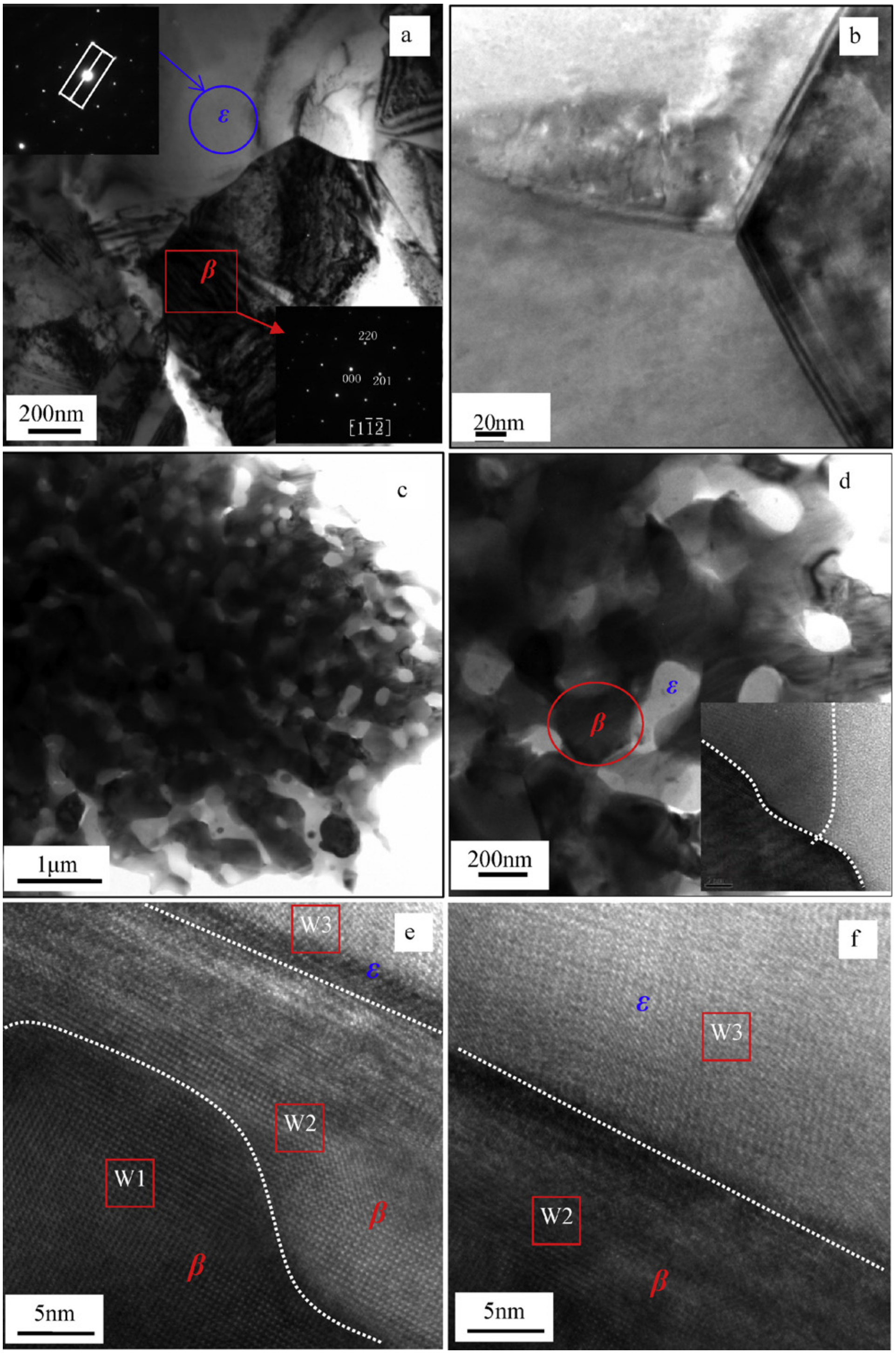

**Fig. 4.** TEM images of the samples: (a and b) HP1100; and (c–f) SPS1100.

gas using computer-controlled equipment. The thermal conductivity was calculated according to the equation $\kappa = C_P D\rho$, where $C_P$ is the specific heat, $D$ is the thermal diffusivity, and $\rho$ is the density of the samples. The $C_P$ and $D$ were measured in flowing argon gas by the laser flash method using Netzsch LFA-427 thermal constant analyzer. The samples for the measurements of thermal transport properties were cut out of the sintered bodies in the form of circular disk of $\Phi = 12.66\,\text{mm} \times 2\,\text{mm}$. The density of the samples was determined by the Archimedes method.

## 3. Results and discussion

An SEM image of the powder sample used for the HP and SPS experiments is shown in Fig. 1a. The particles are homogenously distributed with a mean size about 1 μm. The corresponding XRD pattern indicates that tetragonal α-$Fe_2Si_5$ (JCPDS Card no. 35-0822) and cubic ε-FeSi (JCPDS Card no. 38-1397) phases coexisted in the powder sample (Fig. 1b).

Fig. 2 displays the XRD patterns of the HP and SPS samples. The XRD patterns of all samples are nearly same, but the diffraction peaks shift slightly to the higher angles with hot-pressing temperature decreases from 1100 °C to 880 °C, indicating the following decrease of lattice parameter [15]. Similarly, the lattice parameter of the SPS1100 is smaller than that of the HP1100. In the XRD results, both the orthorhombic β-$FeSi_2$ (JCPDS Card no. 20-0532)

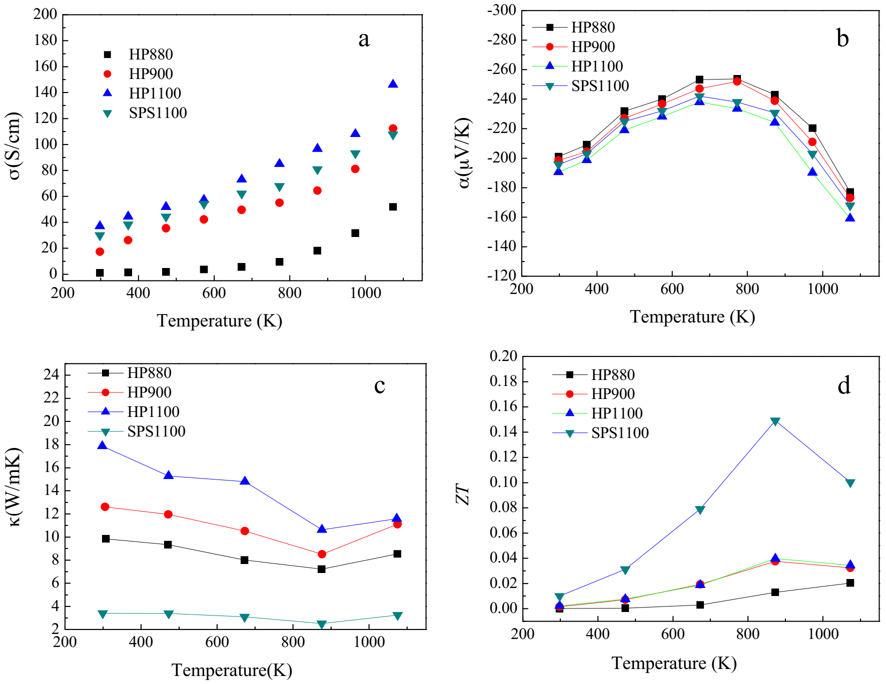

**Fig. 5.** Variable-temperature transport performance of the HP and SPS samples: (a) electrical conductivity; (b) Seebeck coefficient; (c) thermal conductivity; and (d) *ZT*.

and cubic ε-FeSi (JCPDS Card no. 38-1397) phases can be observed, which suggest that α and ε phases are successfully transformed to β phase. It is well known that ε-FeSi phase generally remains stable after normal fabrication procedure [16]. According to ref. [17], the phase transformation during thermal treatment proceeded by the following reaction:

$$\alpha\text{-Fe}_2\text{Si}_5 + \varepsilon\text{-FeSi} \rightarrow 3\beta\text{-FeSi}_2 \qquad (1)$$

Fig. 3 shows the fractural section microstructure of the HP and SPS samples. From Fig. 3a, it can be seen that the density of the HP880 sample is relatively low, and a lot of loose particles with the average sizes of about 1 μm can be observed in the sample. With the increasing hot-pressed temperature to 900 °C (see Fig. 3b), the density of the sample is improved largely and no loose particles are found. However, a few nanopores are observed in the HP900 sample, as shown in the magnified image (the inset in Fig. 3b). As the hot-pressed temperature is further increased to 1100 °C (Fig. 3c), the sample is so dense that no pore or loose particle is observed (the inset in Fig. 3c). For comparison, the microstructure of the SPS1100 is given in Fig. 3d, which is significantly different from that of the HP1100. No loose particle or pore is observed in the SPS1100, while the blurry outlines of the particles can be seen in the inset image of Fig. 3d. These results are in agreement with the measured bulk densities of the samples processed under various conditions. The relative densities of HP880, HP900, HP1100 and SPS1100 are 64%, 87%, 97.8% and 96.5%, respectively.

To confirm the grain sizes and the distribution of β and ε phases, the TEM micrographs of the consolidated samples are carried out. As depicted in Fig. 4, it can be clearly observed that both HP and SPS consolidation processes significantly induce different distributions of the β and ε phases, which is compatible with the densification mechanism. As displayed in Fig. 4a, the selected-area electron diffraction (SAED) patterns indicate that black region is β phase and the gray region is ε phase [18,19]. The β-$FeSi_2$ grains of the HP1100 sample are irregular and with the sizes of about 1 μm. The grain boundary could be clearly observed from the corresponding high-magnification image (Fig. 4b). The growth of β-$FeSi_2$ and ε-FeSi phases is suppressed obviously in the case of the sample consolidated using the SPS process, which is in agreement with ref. [20]. As indicated in Fig. 4c, the bright spherical ε phase is dispersed into the dark β phase matrix during SPS process. It is clearly noted that the grains' sizes of β-$FeSi_2$ and ε-FeSi are about 300 nm and 200 nm, respectively (Fig. 4d). The grain boundary could be clearly observed from the corresponding high-resolution TEM (HRTEM) image, as denoted in white dashed line (the inset in Fig. 4d). The boundaries exist among the same (or different) phases, as shown in Fig. 4e and f, W1 and W2 regions are β-$FeSi_2$ phase, and W3 region is ε-FeSi phase. The result is corresponding to the report from Zhao and co-workers [21]. The difference in the microstructures of the HP and SPS samples lies in the densification mechanism [22].

The electrical conductivity $\sigma$ for all samples shows an increase over the entire temperature range (Fig. 5a). For the hot-pressed samples, electrical conductivity $\sigma$ increases with pressing temperature. This can be explained by the higher densities resulting from high sintering temperature [21], as shown in Fig. 3. However, the $\sigma$ value of the SPS1100 sample is slightly lower than that of the HP1100 sample attributed to the increase in electron scattering.

Fig. 5b shows the temperature dependence of the Seebeck coefficient $\alpha$ between 300 and 1100 K. All these samples exhibiting negative Seebeck coefficient imply *n*-type transport behavior. Below 800 K, Seebeck coefficient increases due to the increase in lattice scattering, and then decreases with temperature owing to a rapid increase in carrier concentration by excitation. Meanwhile, for the hot-pressed samples, the $\alpha$ values decrease with increasing pressing temperature, in conjunction with the associated change of the electrical conductivity behavior shown in Fig. 5a. This can be explained by the stronger scattering on grain boundaries resulting from low sintering temperature. Similarly, the $\alpha$ value of the SPS1100 sample is slightly higher than that of the HP1100 sample owing to the increase in the particle boundaries. However, the Seebeck coefficient is less sensitive to the consolidated process change than the electrical conductivity.

As a function of temperature, the total thermal conductivity $\kappa$ is presented in Fig. 5c. The $\kappa$ value for all the samples decreases monotonously with temperature below 900 K, which is accordant with that of the report for iron disilicide by Zhao and co-workers

[21]. Due to the onset of mixed conduction (holes as well as electrons), the thermal conductivity rises above 1000 K [23]. For the hot-pressed samples, the $\kappa$ values increase with pressing temperature owing to the increase of bulk densities. On the other hand, due to the high boundary scattering, the thermal conductivity of the SPS1100 sample is about 5 times lower than that of the HP1100 sample over the entire temperature range. In the SPS1100 sample, the high boundary scatterings are mainly from fine grains and the dispersion of fine $\varepsilon$ phase in the β phase matrix.

As mentioned, the thermal conductivity composes of electronic and lattice parts. The electronic thermal conductivity can be calculated by the Wiedemann–Franz law [24], $\kappa_e = L\sigma T$, where $L$ is the Lorenz constant with the value of $2.0 \times 10^{-8}\,V^2\,K^{-2}$ used in this study [15,25]. However, the electronic thermal conductivity $\kappa_e$ of the SPS1100 sample (about 0.15 W/(m K) at 873 K) is expected to be negligible in comparison to lattice thermal conductivity $\kappa_l$ ($\kappa_l = \kappa - \kappa_e$), which is about 2.37 W/(m K). Thus, this reduction in total thermal conductivity is almost entirely from the decrement in the lattice thermal conductivity, i.e., the stronger lattice vibration.

Based on the results of the thermoelectric properties, the dimensionless figure of merit, *ZT*, can be calculated for the β-$FeSi_2$ samples obtained by different processes (Fig. 5d). The results reveal that the *ZT* value cannot be improved obviously by increasing pressing temperature due to the high thermal conductivity. While, the SPS process can significantly enhance the figure of merit at high temperature owing to the large reduction in thermal conductivity and the increment in Seebeck coefficient. A maximum *ZT* value of 0.15 is achieved at 873 K for the SPS1100 sample in this work, which is comparable to the results reported in other publications, $ZT \sim 0.18$ for β-$FeSi_2$ doped with 20% $SiO_2$ at about 1073 K [26].

## 4. Conclusions

The β-$FeSi_2$ bulk samples are fabricated by HP and SPS process. The effects of hot-pressing temperature on the microstructures and thermoelectric properties of β-$FeSi_2$ based alloys are investigated. At the same time, the same powder was sintered using SPS method. The effects of the HP and SPS process on the microstructures and thermoelectric properties of β-$FeSi_2$ based alloys are compared. From the experimental results and discussions above, it is drawn as a conclusion that the density of the HP samples increase remarkably and the corresponding TE performance improves slightly with increasing pressing temperature. Besides, the increase of the grain size and the growth of β-$FeSi_2$ and $\varepsilon$-FeSi phases are more limited in SPS process, which leads to existence of more boundaries. Therefore, the SPS1100 sample shows excellent TE performance and the maximum *ZT* value of 0.15 is achieved at 873 K because of the very low thermal conductivity.

## Acknowledgments

We thank the financial supports from National Natural Science Foundation of China (05102041), Programs of Science and Technology Department of Heilongjiang Province (GZ09A404), Education Bureau of Heilongjiang Province (11551118) and Harbin Normal University (KGB201009).

## References

[1] F. Delorme, C.F. Martin, P. Marudhachalam, D.O. Ovono, G. Guzman, J. Alloys Compd. 509 (2011) 2311–2315.
[2] J.F. Li, W.S. Liu, L.D. Zhao, M. Zhou, NPG Asia Mater. 2 (2010) 152–158.
[3] J.Q. Li, S.P. Li, Q.B. Wang, L. Wang, F.S. Liu, W.Q. Ao, J. Alloys Compd. 509 (2011) 4516–4519.
[4] T.C. Harman, P.J. Taylor, M.P. Walsh, B.E. Laforge, Science 297 (2002) 2229–2232.
[5] K. Hattori, Y. Murata, A.N. Hattori, H. Daimon, Vacuum 84 (2010) 648–652.
[6] H. Wu, B. Hu, N. Tian, Q. Zheng, Mater. Lett. 65 (2011) 2877–2879.
[7] Y. Ujiie, K. Nakamori, S. Mashiko, H. Udono, T. Nagata, Phys. Procedia 11 (2011) 177–180.
[8] X.R. Qu, W. Wang, W. Liu, Z.H. Yang, X.M. Duan, D.C. Jia, Mater. Chem. Phys. 129 (2011) 331–336.
[9] Q.S. Meng, W.H. Fan, R.X. Chen, Z.A. Munir, J. Alloys Compd. 492 (2010) 303–306.
[10] X.B. Zhao, H.Y. Chen, E. Mueller, C. Drasar, Appl. Phys. A 80 (2005) 1123–1127.
[11] S.Y. Wang, W.J. Xie, H. Li, X.F. Tang, Intermetallics 19 (2011) 1024–1031.
[12] D.H. Kim, C. Kim, S.H. Heo, H. Kim, Acta Mater. 59 (2011) 405–411.
[13] W.M. Guo, Z.G. Yang, G.J. Zhang, Int. J. Refract. Met. Hard Mater. 29 (2011) 452–455.
[14] W.J. Xie, X.F. Tang, Y.G. Yan, Q.J. Zhang, T.M. Tritt, Appl. Phys. Lett. 94 (2009) 102111.
[15] S.N. Zhang, T.J. Zhu, S.H. Yang, C. Yu, X.B. Zhao, Acta Mater. 58 (2010) 4160–4169.
[16] S.W. Kim, M.K. Cho, Y. Mishima, D.C. Choi, Intermetallics 11 (2003) 399–405.
[17] Y.K. Hsu, J.J. Wang, C.S. Chang, S.C. Wang, Jpn. J. Appl. Phys. 41 (2002) 3854–3859.
[18] N. Otogawa, S. Wang, S. Kihara, Z.X. Liu, Y. Fukuzawa, Y. Suzuki, M. Osamura, T. Ootsuka, T. Mise, K. Nakayama, H. Tanoue, Y. Makita, Thin Solid Films 461 (2004) 223–226.
[19] S.C. Ur, I.H. Kim, Mater. Lett. 57 (2002) 543–551.
[20] M.A. Bousnina, A. Omrani, F. Schoenstein, P. Madec, H. Haddadi, L.S. Smri, N. Jouini, J. Alloys Compd. 5045 (2010) 5323–5327.
[21] H.Y. Chen, X.B. Zhao, C. Stiewe, D. Platzek, E. Mueller, J. Alloys Compd. 433 (2007) 338–344.
[22] G. Bernard-Granger, A. Addad, G. Fantozzi, G. Bonnefont, C. Guizard, D. Vernat, Acta Mater. 58 (2010) 3390–3399.
[23] E.S. Toberer, M. Christensen, B.B. Iversen, G.J. Snyder, Phys. Rev. B 77 (2008) 075203.
[24] A.F. May, J.P. Fleurial, G.J. Snyder, Phys. Rev. B 78 (2008) 125205.
[25] Z. Xiong, X.H. Chen, X.Y. Huang, S.Q. Bai, L.D. Chen, Acta Mater. 58 (2010) 3995–4002.
[26] H. Muta, K. Kurosaki, M. Uno, S. Yamanaka, J. Alloys Compd. 359 (2003) 326–329.